nanomaterials

MDPI

Article

Dimethylglyoxime Clathrate as Ligand Derived Nitrogen-Doped Carbon-Supported Nano-Metal Particles as Catalysts for Oxygen Reduction Reaction

Luping Xu [1,†], Zhongqin Guo [2,†], Hanyu Jiang [1], Siyu Xu [1], Juanli Ma [1], Mi Hu [1], Jiemei Yu [2], Fengqi Zhao [1,*] and Taizhong Huang [2,*]

[1] Science and Technology on Combustion and Explosion Laboratory, Xi'an Modern Chemistry Research Institute, Xi'an 710065, China; sungirlxu5@163.com (L.X.); jianghanyu612@126.com (H.J.); xusy99@163.com (S.X.); mjl_821113@sohu.com (J.M.); amphite@hotmail.com (M.H.)

[2] Shandong Provincial Key Laboratory of Fluorine Chemistry and Chemical Materials, School of Chemistry and Chemical Engineering, University of Jinan, Jinan 250022, China; 17862918959@139.com (Z.G.); chm_yujm@ujn.edu.cn (J.Y.)

* Correspondence: npecc@163.com (F.Z.); chm_huangtz@ujn.edu.cn (T.H.); Tel.: +86-29-88291663 (F.Z.); +86-531-89736103 (T.H.)

† The authors equally contributed to the paper.

Abstract: Nitrogen-doped carbon-supported metal nano-particles show great promise as high-performance catalysts for novel energies, organic synthesis, environmental protection, and other fields. The synergistic effect between nitrogen-doped carbon and metal nano-particles enhances the catalytic properties. Thus, how to effectively combine nitrogen-doped carbon with metal nano-particles is a crucial factor for the synthesis of novel catalysts. In this paper, we report on a facile method to prepare nitrogen-doped carbon-supported metal nano-particles by using dimethylglyoxime as ligand. The nano-particles of Pd, Ni, Cu, and Fe were successfully prepared by the pyrolysis of the corresponding clathrate of ions and dimethylglyoxime. The ligand of dimethylglyoxime is adopted as the source for the nitrogen-doped carbon. The nano-structure of the prepared Pd, Ni, Cu, and Fe particles are confirmed by X-ray diffraction, scanning electron microscopy, and trans-mission electron microscopy tests. The catalytic performances of the obtained metal nano-particles for oxygen reduction reaction (ORR) are investigated by cyclic voltammetry, Tafel, linear sweeping voltammetry, rotating disc electrode, rotating ring disc electrode, and other technologies. Results show that the nitrogen-doped carbon-supported metal nano-particles can be highly efficient catalysts for ORR. The results of the paper exhibit a facile methodology to prepare nitrogen-doped carbon-supported metal nano-particles.

Keywords: dimethylglyoxime; metal nano-particles; nitrogen-doped carbon; catalysts; oxygen reduction reaction

Citation: Xu, L.; Guo, Z.; Jiang, H.; Xu, S.; Ma, J.; Hu, M.; Yu, J.; Zhao, F.; Huang, T. Dimethylglyoxime Clathrate as Ligand Derived Nitrogen-Doped Carbon-Supported Nano-Metal Particles as Catalysts for Oxygen Reduction Reaction. *Nanomaterials* **2021**, *11*, 1329. https://doi.org/10.3390/nano11051329

Academic Editor: Nikos Tagmatarchis

Received: 18 April 2021
Accepted: 11 May 2021
Published: 18 May 2021

1. Introduction

Clean and sustainable energies and technologies, such as water splitting cells, metal-air batteries, and fuel cells, are in great demand due to their merits of high-efficiency, high energy intensity, fast start-up, environmental friendliness, and low operating temperature [1,2]. At present, the carbon-supported metal based nano-particles, such as Pt, Pd, etc., are the major catalysts for fuel cells, which assure the proceeding work of fuel cells. For example, carbon-supported platinum (Pt)-based nano-particles are the state-of-the-art ORR catalysts [3,4]. However, the shortcomings of high-cost, easily-poisoned, and poor-durability have become obstacles to their large-scale applications [5]. Therefore, developing high-performance and low-cost electrocatalysts for ORR is urgent for the widespread applications of fuel cells. Recent studies show that various transition metal based materials, such as single atom catalysis [6], metal-organic frameworks (MOFs)-derived transition

metal sulfide [7], oxide and nitride, etc. [8,9], show great promise to be high-performance catalysts for novel energies. With the deepening understanding of the transition metal-based catalysts, transition metal based nano-particles exhibit great potential to be high performance catalysts for many fields, such as ORR, HER, oxy-gen evolution reaction, etc. In the procedure of transition metal-based catalyst preparation, how to control the size and morphology of metal nano-particles is the key technology.

The RhSi-based nano-particles has reported as catalysts for hydrogen evolution reaction (HER) [10]. In all kinds of methodologies to prepare metal nano-particles, adopting MOFs as intermediates is one of the most feasible methods. MOF-derived nitrogen-doped carbon-based functional materials have been reported as high-performance ORR catalysts due to their unique physical and chemical properties such as large specific surface area, polymetallic sites, etc. [11].

Co-CoO/N-rGO and Ni-NiO/N-rGO were synthesized via a simple annealing of graphene oxide-supported cobalt and nickel salts, respectively [12]. On the other hand, the transitional metal (Fe, Co, Ni) nanoparticles encapsulated in nitrogen-doped carbon nanotubes (M/N-CNTs, M = Fe, Co, Ni) were also synthesized via a solid-state thermal reaction [13]. To prevent the oxidation of metal nano-particles, nano-carbon-based support was derived by the pyrolysis of an organic ligand. The derived carbon can also enhance the conductivity and play a synergistic role in catalysis. Except the synthesis of carbon-supported elemental substances, metal oxides were also obtained from MOFs. For example, Cu_2O nanoparticles were prepared by a facile methodology, which was adopted as catalysts for ORR [14]. The nano-sized $CoFe_2O_4$ also showed high catalytic performance for OER [15]. The nano-sized $CoFe_2O_4$ was obtained from the pyrolysis of prussian blue analog MOFs. The catalytic performance of benchmark Pt-based alloys for ORR could also be improved by tuning particle structures [16]. To modulate the structures of different elemental nano-particles, different ligands have been investigated. Zeolitic imidazolate frameworks (ZIFs) [17] provided materials based on simple zeolite structures using different imidazole analogues. 2-Methylimidazolate is a typical ligand for ZIF-8, which exhibits an interesting nanopore topology formed by four-ring and six-ring ZnN_4 clusters [18]. Trifluoroacetic acid/acetic acid based MOFs were synthesized to enhance CO_2 adsorption and catalytic properties [19]. 1H, 5H-benzo(1,2-d,4,5-d) bistriazole was also adopted as a ligand to prepare FeN_3-based catalysts for the reduction of CO [20]. The synthesis and application of MOFs in electrochemistry fields had been reviewed [11], which clearly pointed out that the MOFs were excellent candidates for a large number of applications. The MOF-based materials have been widely studied and kinds of organic materials have been reported as ligands for MOFs. Until now, the MOFs are usually made from ligands with high price and complex structure. How to simplify the synthesis procedure and decrease the cost of MOFs have attracted great attention. This paper adopts dimethylglyoxime clathrate as the ligand to prepare nitrogen-doped carbon-supported transition metal-based nano-particles as catalysts for ORR. Dimethylglyoxime clathrate has the special characteristics of low decomposition temperature and simple procedure to form coordinate materials. Based on the special characteristics, we select the dimethylglyoxime clathrate as the ligand to prepare nitrogen-doped carbon-supported metal nano-particles as catalysts for ORR.

In this paper, we reported the synthesis of nitrogen-doped carbon-supported metal nano-particles of Fe, Ni, Cu, and Pd from the pyrolysis of the clathrate of corresponding metal ions and dimethylglyoxime ($dmgH_2$) at 350 °C. The structures of the nitrogen-doped carbon-supported metal nano-particles were confirmed by scanning electron microscopy, transmission electron microscopy, and other technologies. As a supplement, the catalysis of the nitrogen-doped carbon-supported Fe, Ni, Cu, and Pd nano-particles for ORR was also investigated. Results showed that the nano-particles have good catalytic performance for ORR. The results of the paper provide a novel way to prepare metal nano-particles at low temperature by the pyrolysis of metal-$dmgH_2$ clathrate.

2. Experimental Section

2.1. Materials Synthesis

Graphene oxide (GO) solution was prepared from natural graphite by a modified Hummers' method, which has been reported before [21]. The dimethylglyoxime, nickel chloride Hexahydrate ($NiCl_2 \cdot 6H_2O$), Cupric Chloride Dihydrate ($CuCl_2 \cdot 2H_2O$), Ferric Chloride Hexahydrate ($FeCl_3 \cdot 6H_2O$), Potassium Hydroxide (KOH), Nafion solution (20 wt%) and ethanol were obtained from Sinopharm Chemical Reagent Co., Ltd (Shanghai, China). The high-purity argon and oxygen gas were purchased from Baode Gas Co Ltd (Jinan, China) Except for the GO solution, the other reagents were analytic purity grade and used without any treatments.

The typical synthesis procedure of nitrogen-doped metal nano-particles is illustrated in Scheme 1, and the obtained materials are named as M@NC.

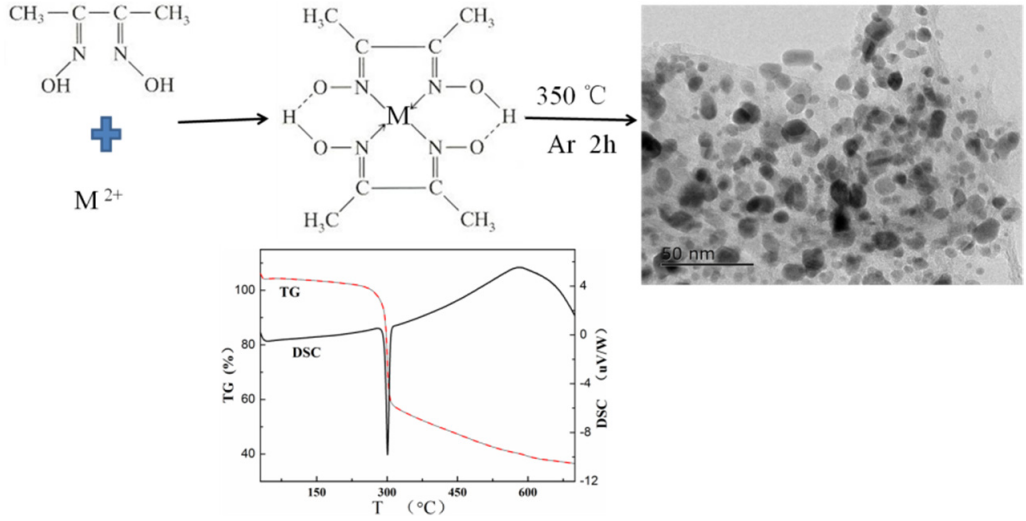

Scheme 1. Illustration of the synthesis of M@NC. The inset is the thermo-gravimetry and differential scanning calorimetry test, which clearly reveals that the pyrolysis of $(dmg)_2M$ clathrate happened at about 300 °C.

The typical synthesis process of Ni@NC is as follows: 1.0015 g $dmgH_2$ was completely dissolved in 100 mL ethanol, and then 2 mL GO (6 g/L) solution was added and stirred until evenly dispersed. Then 1.0303 g nickel chloride hexahydrate ($NiCl_2 \cdot 6H_2O$) was added to the solution by stirring until completely dissolved. The solution turns bright red. The mixed solution was poured into a round bottom flask and the pH adjusted to 8 with NaOH solution. The finally obtained solution was heated and stirred at 85 °C for 30 minutes, then reacted for 2 h at 55 °C. The obtained precipitation was washed with ethanol and de-ionized water. The finally obtained red precipitate was $(dmg)_2Ni$. Finally, the dried $(dmg)_2Ni$ was heated in Ar at 350 °C for 2 h and the obtained black powder was nitrogen-doped carbon-supported Ni nano-particles named as Ni@NC. The temperature was determined according to the TG-DSC test results that displayed in Scheme 1. The TG-DSC tests were conducted by a STA449F3 equipment of Netzsch Co. Ltd (Selb, Gemany). It could be seen from Scheme 1 that the pyrolysis temperature of the coordinate of dimethylglyoxime with metals is about 300 °C. To avoid the growth of metal nano-particles, we selected 350 °C as the final synthesis temperature. The preparation procedure of Fe-, Cu-, and Pd-$(dmg)_2$ was quite similar to that of $(dmg)_2Ni$ and the obtained materials are named as Fe@NC, Cu@NC, and Pd@NC, respectively. Ravi et al. had reported the synthesis of FeCo alloy that was encapsulated by nitrogen-doped carbon nanotube by heating melamine at 950 °C [22].

2.2. Structure Characterization

A Bruker D8 advanced X-Ray diffractometer (XRD) (Bruke DXS, Karlsruhe, German) with Cu-Kα (λ = 1.5418 Å) was used to collect the XRD data between 10° and 80° (2θ). The images of the transmission electron microscopy (TEM), high-resolution TEM (HRTEM) were obtained with a JEOL 2010 unit (Tokyo, Japan). A Perkin Elmer PHI5300 spectrometer with monochromatized Mg Kα radiation (Waltham, MA, USA) was employed to detect the X-ray photoelectron spectroscopy (XPS) of the catalysts.

2.3. Electrochemical Measurements

A mixed solution of 5.0 mg electrocatalysts Ni-NC, 450 μL DI water and 50 μL Nafion solution (20% in weight) was ultrasonicated for 40 min to form a well-dispersed ink. Then, 5 μL of the ink was pipetted onto the surface of the glass-carbon electrode for CV and RDE tests, while 8 μL of the ink was pipetted onto the RRDE test electrode.

The electrochemical tests were conducted by a CHI 760E electrochemical workstation, which is a product of China Shanghai Chenhua Co. Ltd., with a three-electrode cell setup, which included glassy carbon disk (working electrode), carbon electrode (counter electrode), and Ag/AgCl (reference electrode). The cyclic voltammetry (CV), linear sweep voltammetry (LSV), electrochemical impedance spectroscopy (EIS), and Tafel tests were conducted. The CV tests of the materials were conducted in both Ar- and oxygen-saturated 0.1 M KOH electrolyte between 0.2 and −0.8 V (vs. Ag/AgCl) with the sweeping rate of 0.005 V s^{-1}. The LSV, Tafel and EIS tests were also conducted in an O_2-saturated electrolyte. A rotating ring disc electrode (RRDE) and rotating disc electrode (RDE) tests were evaluated at different rotating speeds by a RRDE 3A electrode that combined with a CHI 760E electrochemical workstation. For the RDE test, CV tests were conducted in Ar- and O_2-saturated electrolyte to activate the materials. After that, for the RDE, the LSV tests were conducted at the sweeping rate of 0.005 mV/s with the rotating speed ranged from 625 rpm to 2500 rpm. The RRDE tests were conducted at rotating speeds of 1600 rpm with the same sweeping rate. Based on the RDE tests, the electron transfer number (n) of ORR can be calculated according to the Koutechy–Levich equation (Equation (1)) [23]:

$$\frac{1}{J} = \frac{1}{J_L} + \frac{1}{J_K} = \frac{1}{B\omega^{-1/2}} + \frac{1}{J_K} \quad (1)$$

The slope of the *K-L* line could be written as Equation (2) [7]:

$$B = 0.62nFC_0(D_0)^{2/3}v^{-1/6} \quad (2)$$

where n is the electron transfer number, F is the Faraday constant (96,485 C/mol), D_0 is the diffusion coefficient of O_2 in the electrolyte, v is the kinetic viscosity, and C_0 is the bulk concentration of O_2 in the electrolyte. The constant 0.62 is adopted when the rotating speed ω is expressed in rad/s.

Based on the RRDE tests, the n and percentage ratio of hydrogen peroxide (H_2O_2%) on the electrode surface could be calculated according to Equations (3) and (4) [24]:

$$n = \frac{4 \times I_d}{I_d + I_r/N} \quad (3)$$

$$H_2O_2\% = 200 \times \frac{I_r/N}{I_d + I_r/N} \quad (4)$$

where the value of N is 0.39.

3. Result and Discussions

The structure of the catalysts were firstly investigated by XRD and XPS tests and the results are displayed in Figure 1.

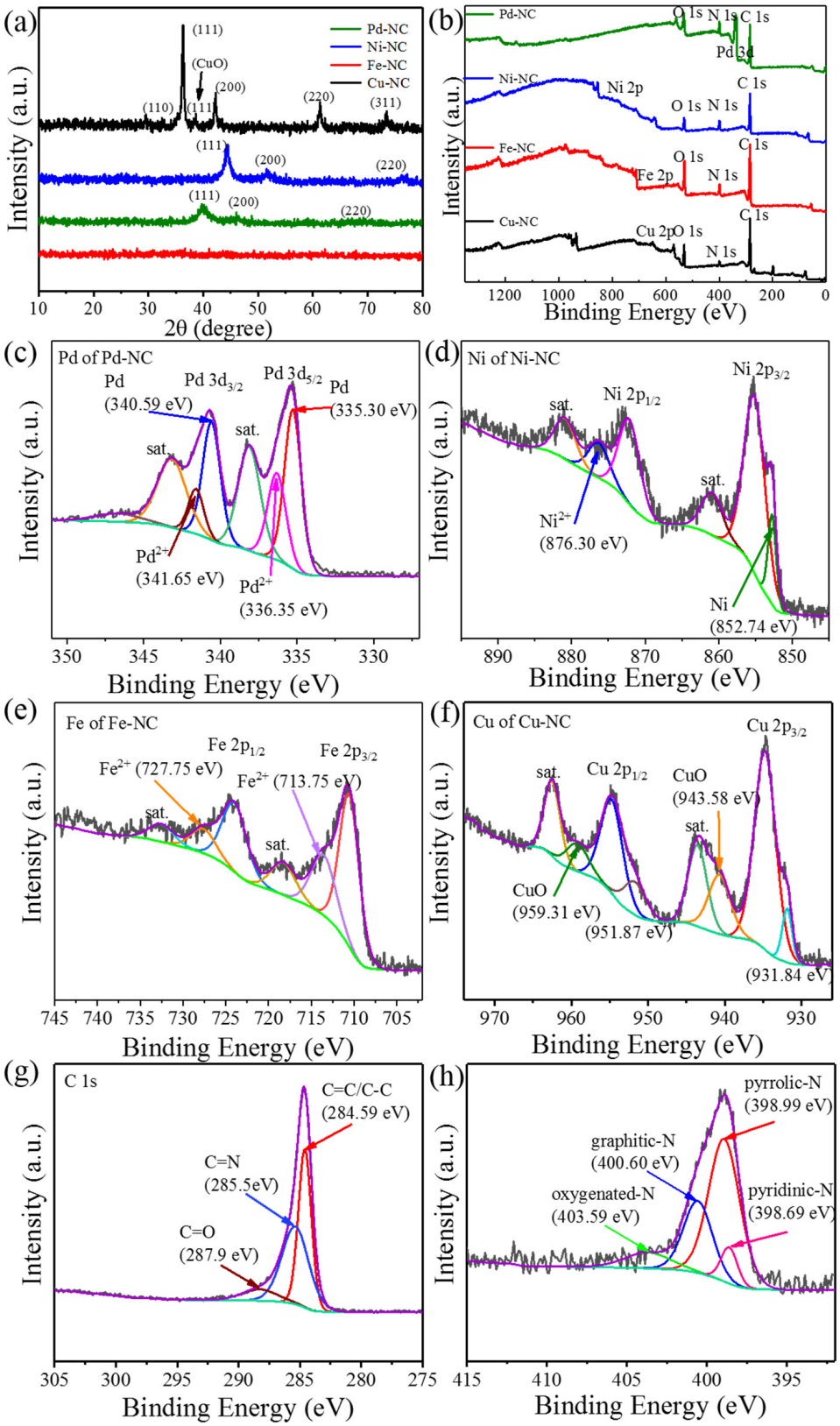

Figure 1. (**a**) XRD patterns of Pd-NC, Ni-NC, Fe-NC, Cu-NC. (**b**) Full spectra of XPS of Pd-NC, Ni-NC, Fe-NC, Cu-NC. High-resolution XPS of Pd of Pd-NC (**c**), Ni of Ni-NC (**d**), Fe of Fe-NC (**e**), Cu of Cu-NC (**f**), C of Pd-NC (**g**), N of Pd-NC (**h**).

The XRD patterns in Figure 1a clearly revealed that the diffraction peaks of Cu-NC were corresponding to the indexed Joint Committee on Powder Diffraction Standards (JCPDS) no. 78-2076 of Cu with micro amount of CuO [14]. The XRD patterns of Ni-NC and Pd-NC were indexed to corresponding to no. 04-1043 and 46-1043, which confirmed the successful synthesis of Ni and Pd nano-particles, respectively. However, to the Fe-NC, no obvious peaks could be indexed, which should be attributed to the Fe particles' size being too small to produce effective diffraction.

To investigate the state of the compositional elements, the X-ray photoelectron spectroscopy (XPS) tests of each catalyst were conducted and the full spectra of the XPS of Ni-, Cu-, Pd-, and Fe-NC are shown in Figure 1b, which clearly proved the successful synthesis of the corresponding materials. The signal of C and N in Figure 1b should be attributed to the $dmgH_2$ derived carbon.

Figure 1c shows the high-resolution XPS of Pd element. The two peaks corresponding to 340.59 and 335.30 eV should belong to the Pd $3d_{3/2}$ and $3d_{5/2}$ [25], which also affirmed the successful synthesis of Pd nano-particles. The existence of Pd^{2+} could be attributed to the partially-oxidized Pd [26], which may be happened during the process of samples preparation for XPS tests. Figure 1d shows the high-resolution XPS of Ni. The two peaks corresponding to 872.43 and 852.74 eV should belong to Ni $2p_{1/2}$ and $2p_{3/2}$, respectively [27]. The existence of Ni^{2+} could be attributed to the NiO [28]. Figure 1e shows the high-resolution XPS of Fe. The two peaks with the binding energy 727.75 and 713.75 eV should be attributed to the $2p_{1/2}$ and $2p_{3/2}$, respectively [29]. The existence of Fe^{2+} could be attributed to the partial oxidized Fe. This clearly proved the successful synthesis of Fe from the coordinate of $(dmg)_2Fe$.

Figure 1f shows the high-resolution XPS of Cu. The peaks with the binding energy of 954.85 and 934.73 eV should belong to the $2p_{1/2}$ and $2p_{3/2}$ of Cu [30], and the peaks of 959.31 and 943.58 eV should belong to the $2p_{1/2}$ and $2p_{3/2}$ of CuO [31]. The XPS test results of Pd-NC, Ni-NC, Cu-NC, and Fe-NC are consistent with the results of XRD tests. The deconvoluted high-resolution XPS of C and N of the materials are quite similar. The typical XPS of C 1s of Pd-NC is shown in Figure 1g. It clearly shows the existence of C=O (287.9 eV), C=N (285.5 eV) and C=C/C–C (284.59 eV) bonds [32]. Figure 1h shows the high-resolution XPS of N 1s. The four peaks spectra in the spectra can be deconvoluted into oxygenated-N (403.59 eV), graphitic-N (400.60 eV), pyrrolic-N (398.99 eV), and pyridinic-N (398.69 eV) [33]. The combined N-C bond proved the successful synthesis of the nitrogen-doped carbon support. Graphitic-N and pyridinic-N are beneficial to the occurrence of ORR. The pyridinic-N has a significant effect on electron delocalization in the carbon framework and, hence, have a profound effect on the ORR performance [34]. The morphology and corresponding elemental mapping of the synthesized materials are displayed in Figure 2.

Figure 2 shows the SEM and corresponding element mapping of the $(dmg)_2$-metal-derived materials. The morphologies of Pd-NC (a), Ni-NC (b), Fe-NC (c), Cu-NC (d) showed that the obtained metal nano-particles evenly distributed on the support, which should be the reduced graphene oxide [35]. The corresponding metal of Pd, Ni, Cu, and Fe should be derived from the clathrate of $(dmg)_2Pd$, $(dmg)_2Ni$, $(dmg)_2Cu$, and $(dmg)_2Fe$. From all the SEM of the obtained materials, it could be seen that the distribution of carbon, nitrogen and metal are consistent with each other, which proved the successful synthesis of the corresponding materials. This result is also consistent with the XRD test results. On the other hand, the ligand-derived nitrogen-doped carbon also prevents the aggregation of derived metal particles, which eventually result in the even distribution of metal particles on the support.

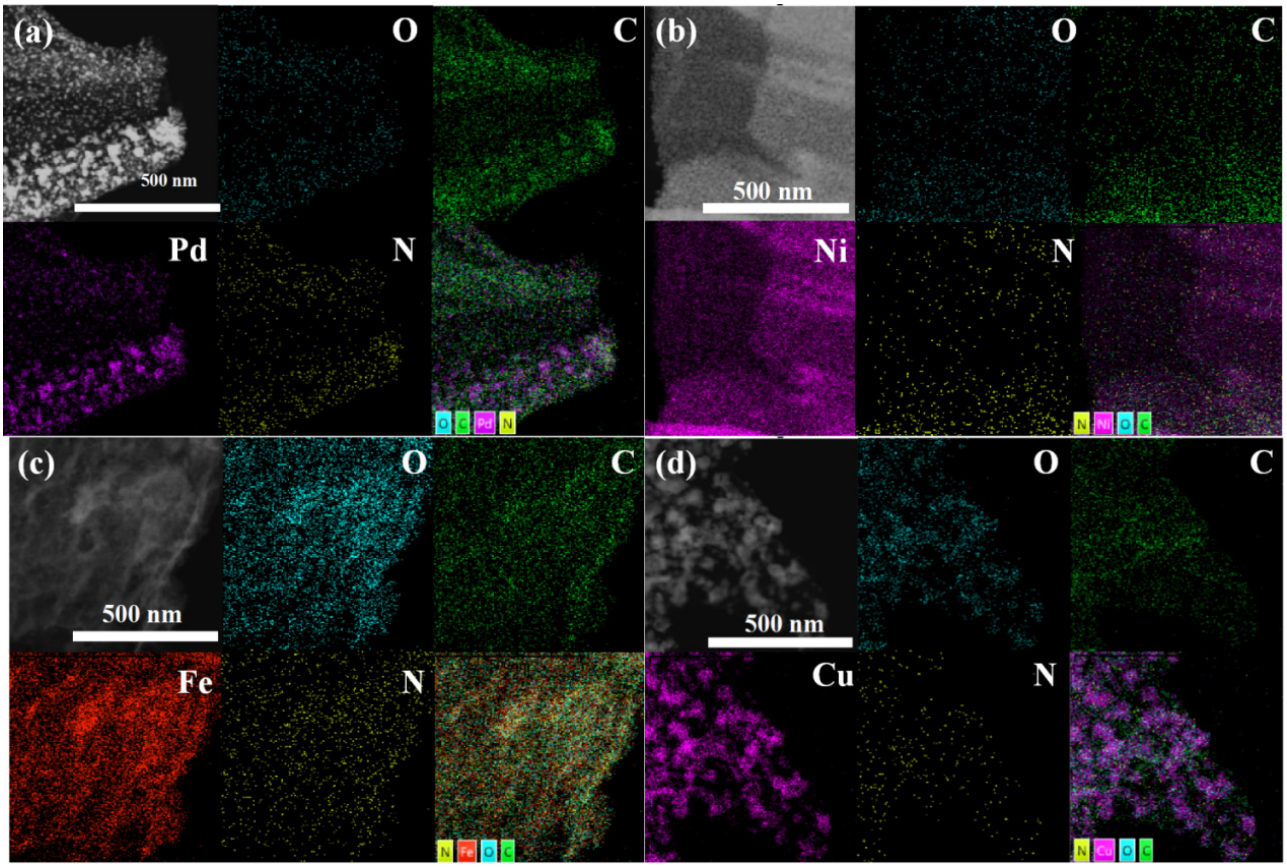

Figure 2. The SEM and corresponding elemental mapping of Pd-NC (**a**), Ni-NC (**b**), Fe-NC (**c**), Cu-NC (**d**).

The HRTEM images of Cu-NC, Fe-NC, Ni-NC, and Pd-NC are shown in Figure 3. The crystal lattice spacing of 0.25 nm, 0.194 nm and 0.173 nm in Figure 3A could correspond to the (111), (200), and (220) facets of Cu. The lattice fringes in Figure 3B confirm the existence of iron rather than amorphous structure. Different lattice distances corresponding to different facets of iron are detected. On the other hand, the SAED patterns also similar to the results of non-crystal materials, which should be attributed to the existence of different lattice facets. The disappearance of obvious XRD patterns should be attributed to the diameter of the particles are too small that make the diffraction of X-ray difficult. In Figure 3C, the crystal lattice spacing of 0.174 nm and 0.206 nm could be attributed to the (200) and (111) facets of Ni. The corresponding SAED patterns also proved the crystal structure of Ni particles [36]. The HRTEM images of Pd in Figure 3D illustrates the crystal lattice spacing of 0.195 nm and 0.239 nm, which matches well with the (111) and (200) facets of Pd. Similar structure was also observed in the research of Pd based catalysts for ORR [37]. The HRTEM results are coincided with the XRD test results. Catalysts with a similar structure were also reported by Vorobyeva et al. [38].

First, the catalytic performances of the materials for ORR were examined by cyclic voltammetry (CV) tests. Figure 4a showed the CV tests of the derived materials at a sweeping rate of 0.005 V/s in both Ar- and O_2-saturated 0.1 M KOH electrolyte. Some obvious peaks were clearly observed in the Figure 4a, which should be attributed to the happening of ORR on the electrode surface. In contrast, it is clearly shown that the onset potential and peak current intensities of ORR of the catalysts are quite different. This should be determined by the intrinsic performance of the derived materials. It is clearly shown that the onset potential of Pd-NC is higher than that of other materials.

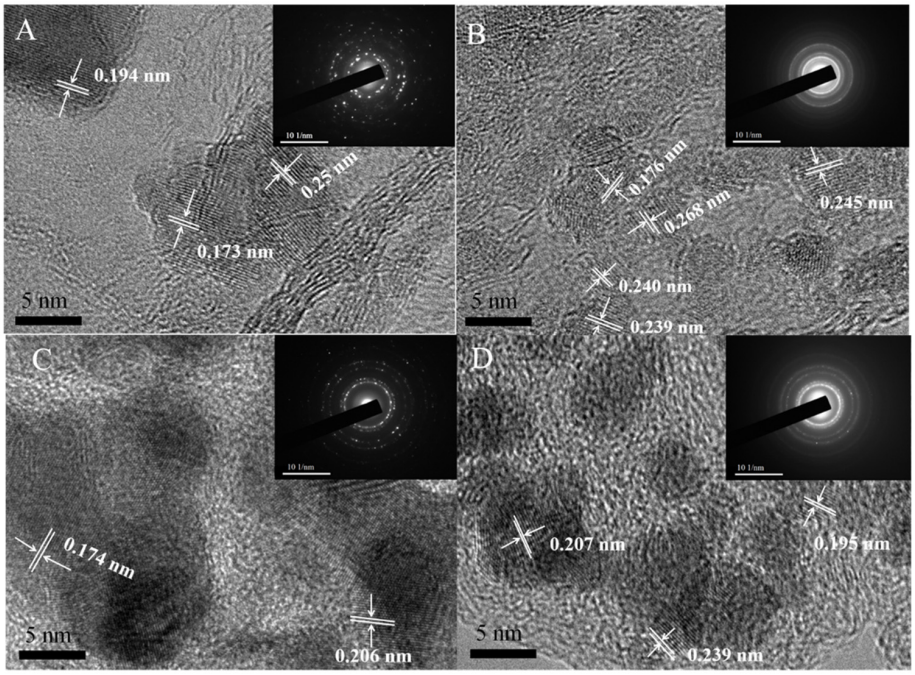

Figure 3. HRTEM tests of Cu-NC (**A**), Fe-NC (**B**), Ni-NC (**C**), Pd-NC (**D**). The inset is the corresponding selected area electron diffraction patterns.

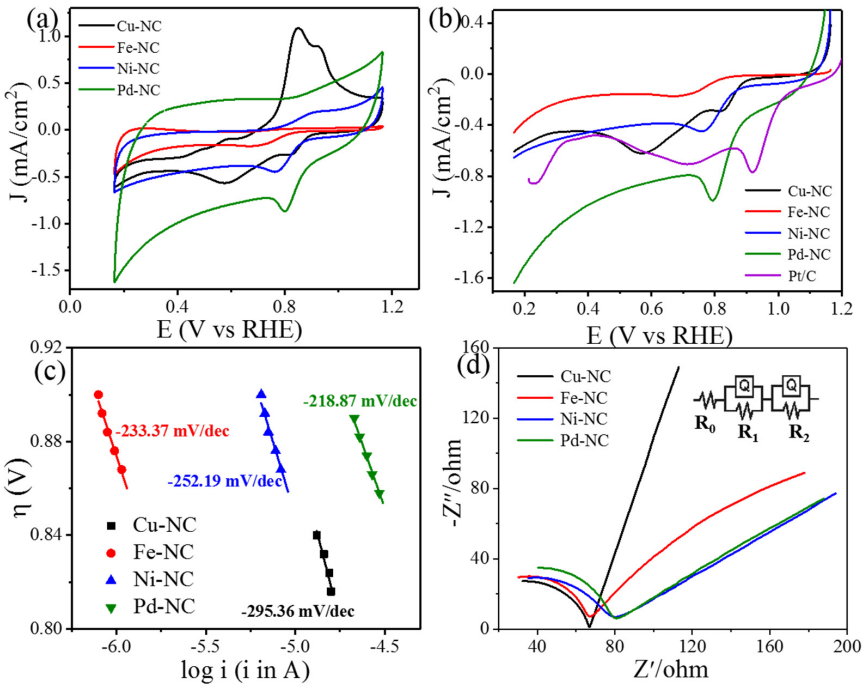

Figure 4. (**a**) CV tests in the oxygen-saturated 0.1 M KOH. LSV (**b**), Tafel (**c**) and EIS (**d**) tests of Pd-NC, Fe-NC, Cu-NC, and Ni-NC in the same electrolyte. As a comparison, the LSV test of Pt/C catalyst is also displayed together.

To further ascertain the catalytic performance of the materials for ORR, the LSV tests of all the materials are conducted and the results are showed in Figure 4b. The onset potential (E_{onset}) and half potential ($E_{1/2}$) of Pd-NC catalyzed ORR are 0.95V, and 0.87 V (vs. RHE), respectively, which is the highest in all the prepared materials. It is also clearly shown that the E_{onset} and $E_{1/2}$ of the derived Cu-NC are 0.93, 0.87 V, that of the Ni-NC are 0.91, 0.84 V, and that of Fe-NC are 0.86, 0.77 V, respectively. Compared with

Pt/C catalyst, the onset potential of Pd-NC is only 0.1 V lower than that of Pt/C catalysts (1.05 V). On the other hand, it is also observed that the limiting current intensity of Pd-NC is about 0.987 mA cm^{-2}, which surpasses that of the Pt/C (Pt 5 wt%) catalyst. The limiting current of the Cu-NC, Ni-NC and Fe-NC catalysts are 0.283, 0.457, and 0.177 mA cm^{-2}, respectively.

Figure 4c showed the Tafel tests of all the obtained materials. The Tafel slopes of Fe-NC, Ni-NC, and Cu-NC were 233.37, 252.19, and 295.36 mV dec^{-1}, respectively. Thus, the Tafel slope of Pd-NC was 218.87 mV dec^{-1}, and a low Tafel slope indicates a lower polarization for the reaction of ORR [39].

Figure 4d showed the electrochemical impedance spectroscopy (EIS) tests of all the catalysts for ORR. The inset in Figure 4d is the modulated equivalent circuit. R_0 is the ohmic resistant, which mainly composed by the ohmic resistant and solution resistance between the working electrode and the reference electrode [40]. R_1 and R_2 represent the reaction resistant, which are usually attributed the direct four-electron reaction and two-electron reaction of ORR. The values of R_0, R_1, and R_2 of each catalyst are displayed in Table 1.

Table 1. R_0, R_1, and R_2 of Cu-NC, Ni-NC, Pd-NC, and Fe-NC catalyzed ORR.

Material	R_0 (Ω)	R_1 (Ω)	R_2 (Ω)
Cu-NC	10	75	1620
Ni-NC	8	72	1580
Pd-NC	7	68	1380
Fe-NC	11	82	1468

Table 1 clearly showed that the resistant of Pd-NC was the lowest, which should be attributed to the high catalytic performance of Pd-NC for ORR. The ohmic resistance of R_1 and R_2 should be resulted from the four-electron and two-electron pathways of ORR in the alkaline electrolyte. To investigate the catalytic mechanism of the obtained materials for ORR, the RDE and RRDE tests of the obtained Pd-NC, Ni-NC, Fe-NC, and Cu-NC in oxygen saturated 0.1 M KOH electrolyte are shown in Figures 5–8, respectively.

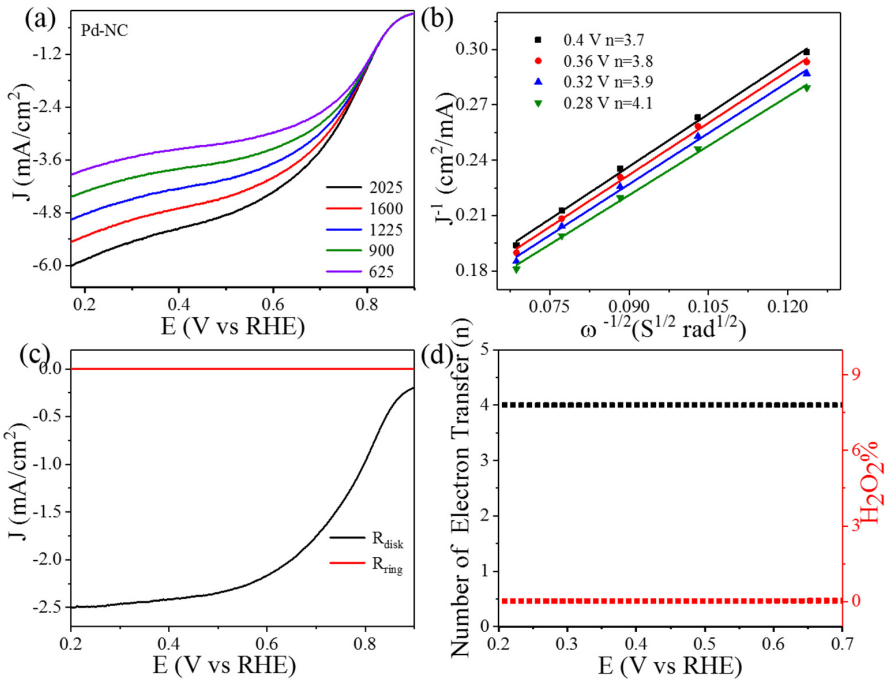

Figure 5. RDE tests (**a**) and corresponding K-L lines (**b**) of Pd-NC in oxygen saturated 0.1 M KOH at various rotation speeds with the sweeping rate of 0.005 V s^{-1}. RRDE test (**c**) and the corresponding electron transfer numbers (*n*) and H_2O_2% (**d**) of Pd-NC at 1600 rpm with the same sweeping rate.

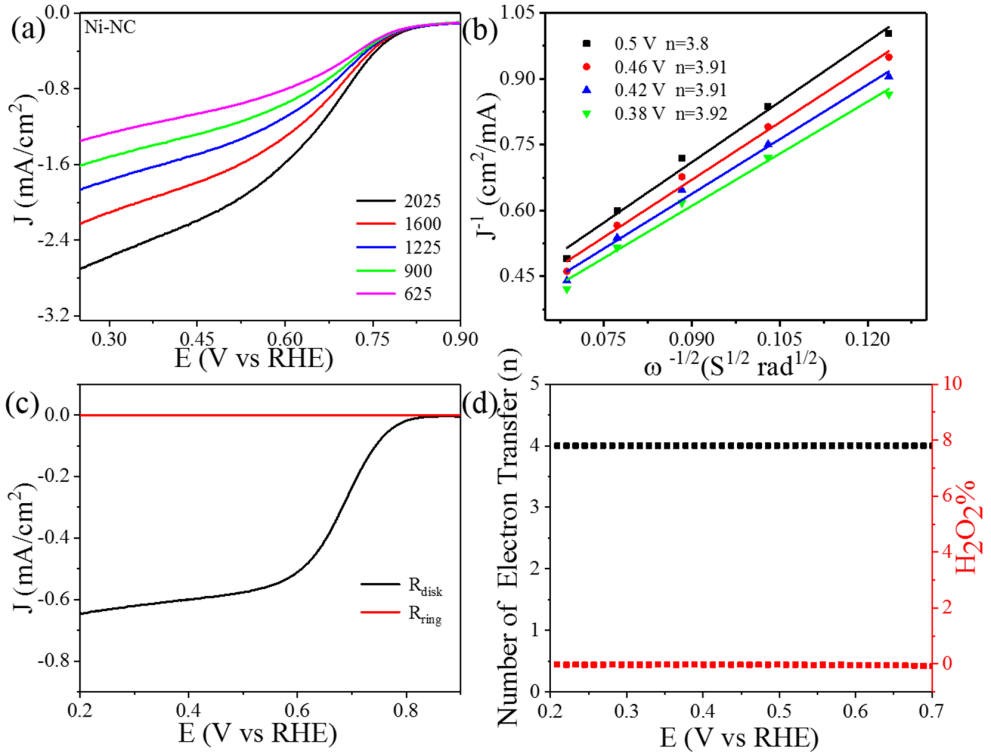

Figure 6. RDE tests (**a**) and corresponding K-L lines (**b**) of Ni-NC in oxygen saturated 0.1 M KOH at various rotation speeds with the sweeping rate of 0.005 V s^{-1}. RRDE test (**c**) and the corresponding electron transfer numbers (*n*) and H_2O_2% (**d**) of Ni-NC at 1600 rpm with the same sweeping rate.

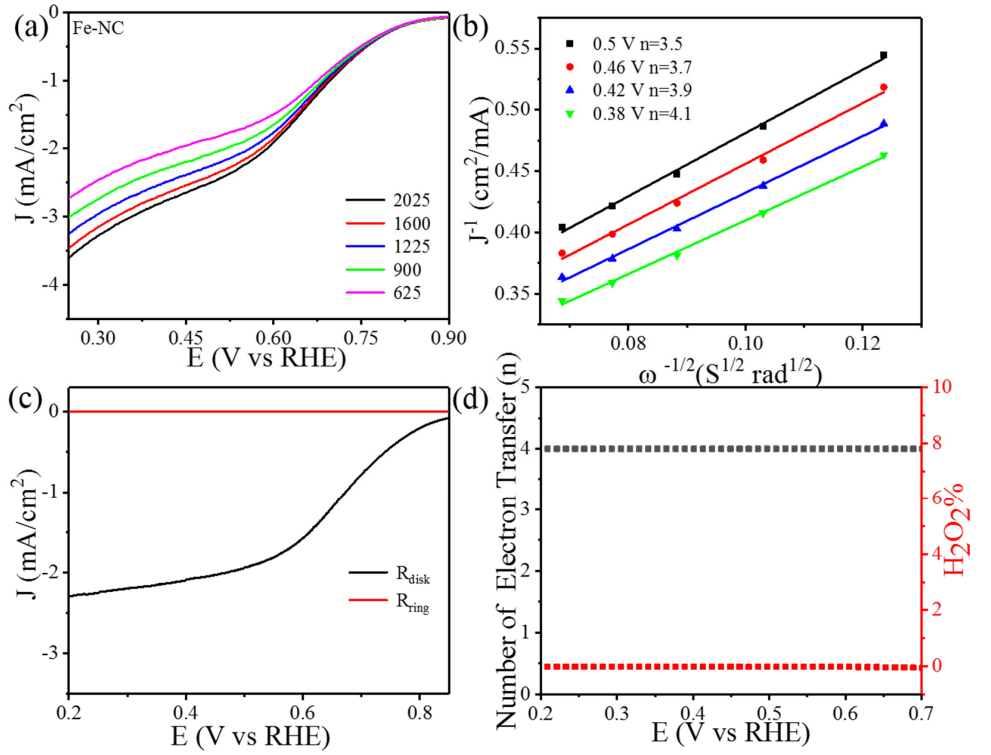

Figure 7. RDE tests (**a**) and corresponding K-L lines (**b**) of Fe-NC in oxygen saturated 0.1 M KOH at various rotation speeds with the sweeping rate of 0.005 V s^{-1}. RRDE test (**c**) and the corresponding electron transfer numbers (*n*) and H_2O_2% (**d**) of Fe-NC at 1600 rpm with the same sweeping rate.

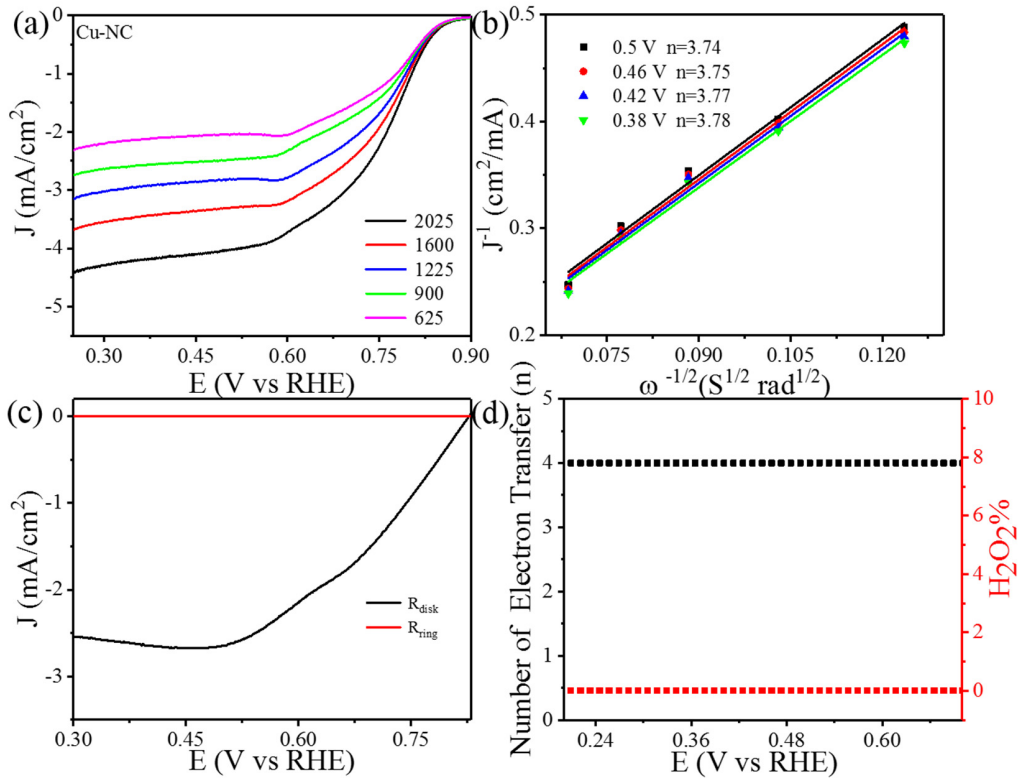

Figure 8. RDE tests (**a**) and corresponding K-L lines (**b**) of Cu-NC in oxygen saturated 0.1 M KOH at various rotation speeds with the sweeping rate of 0.005 V s^{-1}. RRDE test (**c**) and the corresponding electron transfer numbers (*n*) and H_2O_2% (**d**) of Cu-NC at 1600 rpm with the same sweeping rate.

A comparison of the RDE tests of Cu-NC, Ni-NC, Pd-NC and Fe-NC (Figures 5a, 6a, 7a and 8a) showed that, of all the materials, the current intensity increased with increasing rotating speed of the electrode, which should be attributed to the enhanced diffusion rate and shortened diffusion distance of oxygen on the electrode surface [41]. Yu Zhou et al. revealed that the meso-Fe−N−C electrocatalyst with the open porous enables the maximal exposure of highly active for ORR. The coordination between the Fe and nitrogen enhances the catalytic activity and stability for ORR [42].

The *K-L* line in Figures 5b, 6b, 7b and 8b showed the *n* of the obtained materials' catalyzed ORR. It is clearly showed that the value of *n* quite approach to 4. This means that the ORR major happened through the four-electron pathway. The nitrogen-doped carbon-supported metal nano-particles have good catalytic performance for ORR. The ratio of two-electrons on the electrode surface is rather low. A similar phenomena was also observed in the research on nano-cobalt-based catalysts for ORR [43]. The catalytic mechanism of the catalysts for ORR was also investigated by RRDE tests and the results are shown in Figures 5c, 6c, 7c and 8c. All of the diagrams showed that the disc current intensities were much higher than that of the ring electrode. This could be attributed to the high catalytic performance of the materials.

The dependence of the *n* and H_2O_2% on the electrode voltage of Cu-NC, Ni-NC, Pd-NC, and Fe-NC catalyzed ORR are illustrated in Figures 5d, 6d, 7d and 8d, respectively. It is clearly shown that, to the catalysts, the *n* approach 4 and the percentage of H_2O_2% approached 0. This result is quite consistent with the results of the RDE tests. The high catalytic performance should be attributed to the synergistic effect of the metal nano-particles and the nitrogen-doped carbon [44]. The strong chemical attachment and electrical coupling between the electrocatalytic nano-particles and nanocarbon improves the activity and durability of nonprecious metal-based electrocatalysts for ORR [45]. To investigate the

catalytic performance of different alloys, we displayed the catalytic performances of some metals in comparison in Table 2.

Table 2. Comparison of the catalytic performance of Pd with other metals.

Metal	E_0 (V)	I_p (mA/cm^2)	Reference
Pd	0.95	6.0	This work
Zn-N_4	0.905	6.1	[46]
Co-N-C	0.87	5.4	[47]
Ti-O	0.80	5.0	[48]

Table 2 clearly shows that the catalytic performance of Pd-NC is superior to some transition metal-based catalysts despite there also being some other catalysts with higher performances. Compared with the other metal-based catalysts, the preparation temperature of this kind of catalyst is the lowest.

4. Conclusions

In this paper, we report a facile method to prepare nitrogen-doped carbon-supported metal nano-particle-based catalysts for ORR by the pyrolysis of dimethylglyoxime-metal ion clathrate. The dimethylglyoxime is a low-cost ligand for the preparation of MOFs that can be easily loaded onto graphene oxide or other supports. The structure of the obtained materials were examined by XRD, XPS, and HRTEM tests, which proved the successfully synthesized Pd-NC, Fe-NC, Ni-NC, and Cu-NC materials. The catalytic performance of the materials for ORR were examined by CV, LSV, Tafel, EIS, RDE, and RRDE tests, which clearly showed that the all the catalysts showed excellent performance for ORR. On the whole, this paper reported a facile method to prepare nitrogen-doped metal nano-particles as high-performance catalysts. The dimethylglyoxime is an effective ligand to prepare metal nano-particles.

Author Contributions: Conceptualization, L.X., H.J. and F.Z.; methodology, Z.G. and M.H., T.H.; software, Z.G. and M.H.; formal analysis, J.M.; investigation, L.X. and F.Z.; writing—original draft preparation, Z.G.; writing—review and editing, L.X. and J.Y.; supervision, F.Z.; project administration, S.X.; funding acquisition, S.X. and T.H. All authors have read and agreed to the published version of the manuscript.

Funding: This research received no external funding.

Data Availability Statement: Data available on request due to restrictions eg privacy or ethical.

Acknowledgments: This work was financially supported by the National Natural Science Foundation of China (no. 22075290), Shandong Provincial Natural Science Foundation, China (no. ZR2018MB036), the Science Development Project of Shandong Provincial (no. 2017GGX40115).

Conflicts of Interest: The authors declare no conflict of interest.

References

1. Merle, G.; Wessling, M.; Nijmeijer, K. Anion exchange membranes for alkaline fuel cells: A review. *J. Membr. Sci.* **2011**, *377*, 1–35. [CrossRef]
2. Gülzow, E. Alkaline fuel cells. *Fuel Cells* **2004**, *4*, 251–255. [CrossRef]
3. Fang, H.; Huang, T.; Mao, J.; Yao, S.; Dinesh, M.M.; Sun, Y.; Liang, N.; Qi, L.; Yu, J.; Jiang, Z. Investigation on the catalytic performance of reduced-graphene-oxide-interpolated FeS_2 and FeS for oxygen reduction reaction. *ChemistrySelect* **2018**, *3*, 10418–10427. [CrossRef]
4. Pan, J.; Lu, S.; Li, Y.; Huang, A.; Zhuang, L.; Lu, J. High-Performance Alkaline Polymer Electrolyte for Fuel Cell Applications. *Adv. Fun. Mater.* **2010**, *20*, 312–319. [CrossRef]
5. Banham, D.; Feng, F.; Pei, K.; Ye, S.; Birss, V. Effect of carbon support nanostructure on the oxygen reduction activity of Pt/C catalysts. *J. Mater. Chem. A* **2013**, *1*, 2812–2820. [CrossRef]
6. Rivera-Cárcamo, C.; Serp, P. Single atom catalysts on carbon-based materials. *ChemCatChem* **2018**, *10*, 5058–5091. [CrossRef]

7. Gao, M.R.; Jiang, J.; Yu, S.H. Solution-based synthesis and design of late transition metal chalcogenide materials for oxygen reduction reaction (ORR). *Small* **2012**, *8*, 13–27. [CrossRef] [PubMed]
8. Li, J.-S.; Li, S.-L.; Tang, Y.-J.; Han, M.; Dai, Z.-H.; Bao, J.-C.; Lan, Y.-Q. Nitrogen-doped Fe/Fe_3C@graphitic layer/carbon nanotube hybrids derived from MOFs: Efficient bifunctional electrocatalysts for ORR and OER. *Chem. Commun.* **2015**, *51*, 2710–2713. [CrossRef] [PubMed]
9. Xiao, M.; Zhu, J.; Li, G.; Li, N.; Li, S.; Cano, Z.P.; Ma, L.; Cui, P.; Xu, P.; Jiang, G.; et al. A single-atom iridium heterogeneous catalyst in oxygen reduction reaction. *Angew. Chem. Int. Ed.* **2019**, *58*, 9640–9645. [CrossRef]
10. Lei, C.; Wang, Y.; Hou, Y.; Liu, P.; Yang, J.; Zhang, T.; Zhuang, X.; Chen, M.; Yang, B.; Lei, L.; et al. Efficient alkaline hydrogen evolution on atomically dispersed Ni–Nx Species anchored porous carbon with embedded Ni nanoparticles by accelerating water dissociation kinetics. *Energy Environ. Sci.* **2019**, *12*, 149–156. [CrossRef]
11. Wu, G.; More, K.L.; Johnston, C.M.; Zelenay, P. High-performance electrocatalysts for oxygen reduction derived from polyaniline, iron, and cobalt. *Science* **2011**, *332*, 443–447. [CrossRef]
12. Liu, X.; Liu, W.; Ko, M.; Park, M.; Kim, M.G.; Oh, P.; Chae, S.; Park, S.; Casimir, A.; Wu, G.; et al. Metal (Ni, Co)-metal oxides/graphene nanocomposites as multifunctional electrocatalysts. *Adv. Fun. Mater.* **2015**, *25*, 5799–5808. [CrossRef]
13. Liu, Y.; Jiang, H.; Zhu, Y.; Yang, X.; Li, C. Transition metals (Fe, Co, and Ni) encapsulated in nitrogen-doped carbon nanotubes as bi-functional catalysts for oxygen electrode reactions. *J. Mater. Chem. A* **2016**, *4*, 1694–1701. [CrossRef]
14. Yan, X.Y.; Tong, X.L.; Zhang, Y.F.; Han, X.D.; Wang, Y.Y.; Jin, G.Q.; Qin, Y.; Guo, X.Y. Cuprous oxide nanoparticles dispersed on reduced graphene oxide as an efficient electrocatalyst for oxygen reduction reaction. *Chem. Commun.* **2012**, *48*, 1892–1894. [CrossRef]
15. Wang, J.; Huang, Z.; Liu, W.; Chang, C.; Tang, H.; Li, Z.; Chen, W.; Jia, C.; Yao, T.; Wei, S.; et al. Design of N-coordinated dual-metal sites: A stable and active Pt-free catalyst for acidic oxygen reduction reaction. *J. Am. Chem. Soc.* **2017**, *139*, 17281–17284. [CrossRef] [PubMed]
16. Guo, S.; Zhang, S.; Sun, S. Tuning Nanoparticle Catalysis for the Oxygen Reduction Reaction. *Angew. Chem. Int. Ed.* **2013**, *52*, 8526–8544. [CrossRef]
17. Ma, Z.; Dou, S.; Shen, A.; Tao, L.; Dai, L.; Wang, S. Sulfur-doped graphene derived from cycled lithium-sulfur batteries as a metal-free electrocatalyst for the oxygen reduction reaction. *Angew. Chem. Int. Ed. Engl.* **2015**, *54*, 1888–1892. [CrossRef]
18. Li, T.; Liu, J.; Song, Y.; Wang, F. Photochemical solid-phase synthesis of platinum single atoms on nitrogen-doped carbon with high loading as bifunctional catalysts for hydrogen evolution and oxygen reduction reactions. *ACS Catal.* **2018**, *8*, 8450–8458. [CrossRef]
19. Sun, Y.; Shen, Z.; Xin, S.; Ma, L.; Xiao, C.; Ding, S.; Li, F.; Gao, G. Ultrafine Co-doped ZnO nanoparticles on reduced graphene oxide as an efficient electrocatalyst for oxygen reduction reaction. *Electrochim. Acta* **2017**, *224*, 561–570. [CrossRef]
20. Li, Q.K.; Li, X.F.; Zhang, G.; Jiang, J. Cooperative spin transition of monodispersed FeN_3 sites within graphene induced by CO adsorption. *J. Am. Chem. Soc.* **2018**, *140*, 15149–15152. [CrossRef]
21. Hummers, W.S., Jr.; Offeman, R.E. Preparation of graphitic oxide. *J. Am. Chem. Soc.* **1958**, *80*, 1339. [CrossRef]
22. Nandan, R.; Pandey, P.; Gautam, A.; Bisen, O.Y.; Chattopadhyay, K.; Titirici, M.-M.; Nanda, K.K. Atomic Arrangement Modulation in CoFe Nanoparticles Encapsulated in N-Doped Carbon Nanostructures for Efficient Oxygen Reduction Reaction. *ACS Appl. Mater. Interfaces* **2021**, *13*, 3771–3781. [CrossRef]
23. Meganathan, M.D.; Mao, S.; Huang, T.; Sun, G. Reduced graphene oxide intercalated Co_2C or Co_4N nanoparticles as an efficient and durable fuel cell catalyst for oxygen reduction. *J. Mater. Chem. A* **2017**, *5*, 2972–2980. [CrossRef]
24. Bayati, M.; Scott, K. Synthesis and Activity of A Single Active Site N-doped Electro-catalyst for Oxygen Reduction. *Electrochim. Acta* **2016**, *213*, 927–932. [CrossRef]
25. Liu, Y.; McCue, A.J.; Miao, C.; Feng, J.; Li, D.; Anderson, J.A. Palladium phosphide nanoparticles as highly selective catalysts for the selective hydrogenation of acetylene. *J. Catal.* **2018**, *364*, 406–414. [CrossRef]
26. Hickman, A.J.; Sanford, M.S. High-valent organometallic copper and palladium in catalysis. *Nature* **2012**, *484*, 177–185. [CrossRef]
27. He, D.; Zhang, L.; He, D.; Zhou, G.; Lin, Y.; Deng, Z.; Hong, X.; Wu, Y.; Chen, C.; Li, Y. Amorphous nickel boride membrane on a platinum–nickel alloy surface for enhanced oxygen reduction reaction. *Nat. Commun.* **2015**, *7*, 12362–12369.
28. Ci, S.; Huang, T.; Wen, Z.; Cui, S.; Mao, S.; Steeber, D.A.; Chen, J. Nickel oxide hollow microsphere for non-enzyme glucose detection. *Biosens. Bioelectron.* **2014**, *54*, 251–257. [CrossRef] [PubMed]
29. Yu, L.; Zhou, H.; Sun, J.; Qin, F.; Yu, F.; Bao, J.; Yu, Y.; Chen, S.; Ren, Z. Cu nanowires shelled with NiFe layered double hydroxide nanosheets as bifunctional electrocatalysts for overall water splitting. *Energy Environ. Sci.* **2017**, *10*, 1820–1827. [CrossRef]
30. Ammon, C.; Bayer, A.; Held, G.; Richter, B.; Schmidt, T.; Steinruck, H.P. Dissociation and oxidation of methanol on Cu(110). *Surf. Sci.* **2002**, *507*, 845–850. [CrossRef]
31. Amin, R.S.; Hameed, R.M.A.; El-Khatib, K.M.; El-Abd, H.; Souaya, E.R. Effect of preparation conditions on the performance of nano Pt-CuO/C electrocatalysts for methanol electro-oxidation. *Int. J. Hydrogen Energy* **2012**, *37*, 18870–18881. [CrossRef]
32. Zhang, Z.; Zhang, Y.; Mu, X.; Du, J.; Wang, H.; Huang, B.; Zhou, J.; Pan, X.; Xie, E. The carbonization temperature effect on the electrochemical performance of nitrogen-doped carbon monoliths. *Electrochim. Acta* **2017**, *242*, 100–106. [CrossRef]
33. Hu, B.-C.; Wu, Z.-Y.; Chu, S.-Q.; Zhu, H.-W.; Liang, H.-W.; Zhang, J.; Yu, S.-H. SiO_2-protected shell mediated templating synthesis of Fe–N-doped carbon nanofibers and their enhanced oxygen reduction reaction performance. *Energy Environ. Sci.* **2018**, *11*, 2208–2215. [CrossRef]

34. Jena, H.S.; Krishnaraj, C.; Parwaiz, S.; Lecoeuvre, F.; Schmidt, J.; Pradhan, D.; Van Der Voort, P. Illustrating the role of quaternary-N of BINOL covalent triazine-based frameworks in oxygen reduction and hydrogen evolution reactions. *ACS Appl. Mater. Interfaces* **2020**, *12*, 44689–44699. [CrossRef] [PubMed]
35. Xu, H.; Cheng, D.; Cao, D.; Zeng, X.C. A universal principle for a rational design of single-atom electrocatalysts. *Nat. Catal.* **2018**, *1*, 339–348. [CrossRef]
36. Li, Y.; Li, F.-M.; Meng, X.-Y.; Wu, X.-R.; Li, S.-N.; Chen, Y. Direct chemical synthesis of ultrathin holey iron doped cobalt oxide nanosheets on nickel foam for oxygen evolution reaction. *Nano Energy* **2018**, *54*, 238–250. [CrossRef]
37. Xue, Q.; Bai, J.; Han, C.; Chen, P.; Jiang, J.-X.; Chen, Y. Au nanowires@Pd-polyethylenimine nanohybrids as highly active and methanol-tolerant electrocatalysts toward oxygen reduction reaction in alkaline media. *ACS Catal.* **2018**, *8*, 11287–11295. [CrossRef]
38. Vorobyeva, E.; Fako, E.; Chen, Z.; Collins, S.M.; Johnstone, D.; Midgley, P.A.; Hauert, R.; Safonova, O.V.; Vilé, G.; López, N.; et al. Atom-by-atom resolution of structure-function relations over low-nuclearity metal catalysts. *Angew. Chem. Int. Ed. Engl.* **2019**, *58*, 8724–8729. [CrossRef]
39. Chen, Y.; Gokhale, R.; Serov, A.; Artyushkova, K.; Atanassov, P. Novel highly active and selective Fe-N-C oxygen reduction electrocatalysts derived from in-situ polymerization pyrolysis. *Nano Energy* **2017**, *38*, 201–209. [CrossRef]
40. Guo, H.-L.; Su, P.; Kang, X.; Ning, S.-K. Synthesis and characterization of nitrogen-doped graphene hydrogels by hydrothermal route with urea as reducing-doping agents. *J. Mater. Chem. A* **2013**, *1*, 2248–2255. [CrossRef]
41. Liang, Y.; Li, Y.; Wang, H.; Zhou, J.; Wang, J.; Regier, T.; Dai, H. Co_3O_4 nanocrystals on graphene as a synergistic catalyst for oxygen reduction reaction. *Nat. Mater.* **2011**, *10*, 780–786. [CrossRef] [PubMed]
42. Zhou, Y.; Yu, Y.; Ma, D.; Foucher, A.C.; Xiong, L.; Zhang, J.; Stach, E.A.; Yue, Q.; Kang, Y. Atomic Fe Dispersed Hierarchical Mesoporous Fe–N–C Nanostructures for an Efficient Oxygen Reduction Reaction. *ACS Catal.* **2020**, *11*, 74–81. [CrossRef]
43. Liang, Y.; Wang, H.; Diao, P.; Chang, W.; Hong, G.; Li, Y.; Gong, M.; Xie, L.; Zhou, J.; Wang, J.; et al. Oxygen reduction electrocatalyst based on strongly coupled cobalt oxide nanocrystals and carbon nanotubes. *J. Am. Chem. Soc.* **2012**, *134*, 15849–15857. [CrossRef]
44. Bezerra, C.W.B.; Zhang, L.; Lee, K.; Liu, H.; Marques, A.L.B.; Marques, E.P.; Wang, H.; Zhang, J. A review of Fe–N/C and Co–N/C catalysts for the oxygen reduction reaction. *Electrochim. Acta* **2008**, *53*, 4937–4951. [CrossRef]
45. Liang, Y.; Li, Y.; Wang, H.; Dai, H. Strongly coupled inorganic/nanocarbon hybrid materials for advanced electrocatalysis. *J. Am. Chem. Soc.* **2013**, *135*, 2013–2036. [CrossRef] [PubMed]
46. Jiang, R.; Chen, X.; Liu, W.; Wang, T.; Qi, D.; Zhi, Q.; Liu, W.; Li, W.; Wang, K.; Jiang, J. Atomic Zn Sites on N and S Codoped Biomass-Derived Graphene for a High-Efficiency Oxygen Reduction Reaction in both Acidic and Alkaline Electrolytes. *ACS Appl. Energy Mater.* **2021**, *4*, 2481–2488. [CrossRef]
47. Yang, S.; Yu, Y.; Dou, M.; Zhang, Z.; Wang, F. Edge-functionalized polyphthalocyanine networks with high oxygen reduction reaction activity. *J. Am. Chem. Soc.* **2020**, *142*, 17524–17530. [CrossRef]
48. Chisaka, M.; Xiang, R.; Maruyama, S.; Daiguji, H. Efficient phosphorus doping into the surface oxide layers on TiN to enhance oxygen reduction reaction activity in acidic media. *ACS Appl. Energy Mater.* **2020**, *3*, 9866–9876. [CrossRef]